International Journal of Applied Engineering Research ISSN 0973-4562 Volume 14, Number 15 (2019) pp. 3464-3471

Heat Balance Integral Solution of Solidification Process of a Liquid over a Rotating Cylinder

Mustafa H. Almadih[*], R.V. Seeniraj[**], Kannan Premnath[+], and Fan-Bill Cheung[*]

[*]*Department of Mechanical Engineering, Pennsylvania State University, State College, PA 16802.*

[+]*Department of Mechanical Engineering, University of Colorado Denver, Denver, CO 80204.*

[**]*Department of Mechanical Engineering, Anna University, Chennai 600025, India.*

Abstract

Phase change involving solidification over a rotating cylinder has a number of applications in engineering especially those involving casting processes in manufacturing and ice production. Due to the nonlinear and coupled nature of such free boundary problems, only approximate analytical or numerical approaches allow their quantitative studies. In this paper, the Heat Balance Integral (HBI) method, with suitable prescription of the temperature profile in the solid and liquid phase regions, is used to determine the evolution of the solidification front. The effects of various characteristic dimensionless parameters on the solidification process over a rotating cylinder are presented.

Keywords: Solidification process, Heat balance integral solution

1. Introduction

Phase change processes such as solidification or melting are common in nature and occur in many situations of engineering interest. In particular, predicting the rate of solidification is important in various manufacturing applications involving casting of metals and processing of plastics and polymers. Exact analytical solutions for phase change problems characterized by the motion of free boundaries are restricted to highly idealized conditions such as those developed by Neumann. Hence approximate analytical or numerical methods play an important role in solving complex free boundary problems.

Among the different approximate analytical approaches, one of the most important and widely used is the so-called Heat Balance Integral (HBI) method developed by Goodman (1958). The approach was refined later by Goodman and Shea (1960) and Goodman (1961) for phase change and other non-linear heat conduction problems. The HBI method is an extension of the integral method proposed and applied to fluid mechanics problems by von Karman and Pohlhausen to heat transfers problems by Goodman and others. For example, Lunardini (1981) applied the HBI method for solidification over a cylinder. The validity of the HBI method for such problems was confirmed later experimentally by Stewart and Smith (1987). Recent applications of the HBI method to various phase change problems are presented, for example, in Refs.[8,10,11,14]. See also Ref.[9] for a review of this method. An interesting physical problem involves the determination of the solidification of a liquid over a rotating cylinder. From a technological context, such a scenario can occur, for example, in the spin casting of metals and plastics. As another example, production of ice in an industrial scale involves freezing of water over a rotating cylindrical drum. In addition, the above problem also has relevance in propulsion applications involving ice accretion over aircraft components. A related problem was considered in Ref.[5]. The aim of the present study is to model and investigate the solidification process over a rotating cylinder. The Heat Balance Integral (HBI) method using a suitable approximation for the temperature profile in cylindrical coordinates will be employed in this work. The application of this method will reduce the energy conservation equation to a simplified ordinary differential equation for the solidification front. Numerical investigation will then be performed to determine the influence of the various characteristic parameters on the evolution of the solidification front. The approach, presently developed for Newtonian fluids, can be extended for solidification of non-Newtonian fluids [12] in a future work.

2. Mathematical Modeling

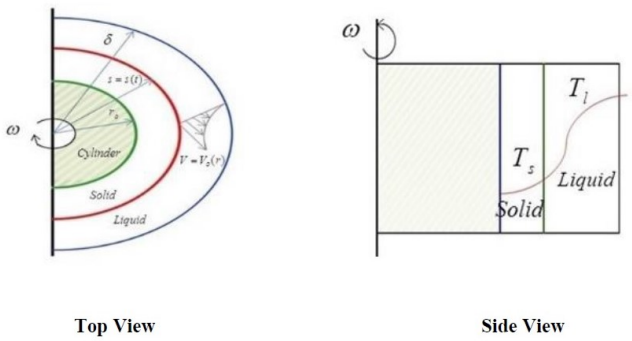

Figure 1:: Schematic diagram of the solidification of a liquid over a rotating cylinder

Figure 1 shows the schematic of the main geometric and physical features for the solidification process over a rotating

cylinder.It consists of a cylinder of radius r_o where the surface is maintained at a temperature T_w and rotating at an angular velocity ω. The cylinder is surrounded by an initially warmer Newtonian liquid at a temperature T_o. Since the cylinder surface temperature T_w is maintained lower than the freezing temperature T_i, the liquid adjacent to the cylinder starts to solidify and the evolution of the radius of the freezing front is represented by $s(t)$.The rotation of the cylinder induces a circumferential fluid motion, where the velocity is represented by $V(r)$. The influence of the thermal effects is felt over a finite radial distance , which is used in the HBI formulation discussed later. The temperature profiles within the solid and liquid regions are denoted by $T_s(r)$ and $T_l(r)$, respectively. The main objective of the present work is the determination of the evolution of the solidification front $s(t)$ using the HBI method.

2.1. Governing Equations for Solid Layer

The mathematical formulation of the outward solidification will now be discussed. The energy conservation, i.e., the heat conduction equation within the solid region is represented by

$$\frac{1}{r}\frac{\partial}{\partial r}\left(\frac{\partial T_s}{\partial r}\right)=\frac{1}{\alpha_s}\frac{\partial T_s}{\partial t}, r_o \le r \le s \tag{1}$$

which is subject to the following boundary conditions:

$$T_s(s,t)=T_i \tag{1.a}$$

$$T_s(r_o,t)=T_w \tag{1.b}$$

2.2. Governing Equations for Liquid Layer

Continuity equation:

$$\frac{1}{r}\frac{\partial V}{\partial \theta}=0 \tag{2}$$

Momentum equation:

$$\frac{\partial^2 V}{\partial r^2}+\frac{\partial}{\partial r}\left(\frac{V}{r}\right)=0 \tag{3}$$

Energy equation: Assuming viscous dissipation in the rotating fluid, the energy equation can be written as:

$$\frac{1}{r}\frac{\partial}{\partial r}\left(r\frac{\partial T_l}{\partial r}\right)+\frac{\mu_l}{K_l}\left[r\frac{\partial}{\partial r}\left(\frac{V}{r}\right)^2\right]=\frac{1}{\alpha_l}\frac{\partial T_l}{\partial t} \tag{4}$$

subject to:

$$T_l(s,t)=T_i \tag{4.a}$$

$$T_l(\delta,t)=T_o \tag{4.b}$$

$$\frac{\partial T_l}{\partial r}(\delta,t)=0 \tag{4.c}$$

$$V(r=s)=\omega s \tag{4.d}$$

$$V(r=\delta)=0 \tag{4.e}$$

2.3. Phase Change Interface (Stefan) Condition

The energy transport between solid and liquid layers is coupled through the interface equation which is also known as the Stefan condition and is given by:

$$K_s\frac{\partial T_s}{\partial r}-K_l\frac{\partial T_l}{\partial r}=\rho_s L\frac{\partial s}{\partial t}, at\ r=s \tag{5}$$

where the first term of the equation represents the heat transfer into solid. The second term represents the heat transfer into the liquid. The term on the right side represents the latent heat absorbed during the solidification process. Effectively, this equation governs the evolution of the solidification front s(t). For convenience, we will now non-dimensionalize the governing equations using the definition of variables given in the Nomenclature section. These are given as follows.

2.4. Normalized Equations for Solid Layer

$$\frac{1}{r^*}\frac{\partial}{\partial r^*}\left(r^*\frac{\partial \theta_s}{\partial r^*}\right)=Ste\frac{\partial \theta_s}{\partial \tau} \tag{6}$$

subject to:

$$\theta_S(\beta,\tau)=1 \tag{6.a}$$

$$\theta_S(1,\tau)=0 \tag{6.b}$$

2.5. Normalized Equations for Liquid Layer

Continuity Equation:

$$\frac{1}{r}\frac{\partial V^*}{\partial \theta}=0, i.e.,\ V^*=V^*(r^*) \tag{7}$$

Momentum Equation:

$$\frac{\partial^2 V^*}{\partial r^{*2}}+\frac{\partial}{\partial r^*}\left(\frac{V^*}{r^*}\right)=0 \tag{8}$$

subject to:

$$V^*(r^*=\beta)=\beta \tag{8.a}$$

$$V^*(r^*=\delta^*)=0 \tag{8.b}$$

Energy Equation:

$$\frac{1}{r^*}\frac{\partial}{\partial r^*}\left(r^*\frac{\partial \theta_l}{\partial r^*}\right)+Ec.Pr\left[r^*\frac{\partial}{\partial r^*}\left(\frac{V^*}{r^*}\right)^2\right]=\frac{\alpha_s}{\alpha_l}Ste\frac{\partial \theta_l}{\partial \tau} \tag{9}$$

subject to:

$$\theta_l(\beta,\tau)=0 \tag{9.a}$$

$$\theta_l(\delta^*,\tau)=1 \tag{9.b}$$

$$\frac{\partial}{\partial r^*}\theta_l(\delta^*,\tau)=0 \tag{9.c}$$

Interface (Stefan) Condition.

$$\frac{\partial \theta_s}{\partial r^*}-\phi\frac{K_l}{K_s}\frac{\partial \theta_l}{\partial r^*}=\frac{\partial \beta}{\partial \tau}, at\ r^*=\beta \tag{10}$$

2.6. Heat Balance Integral Solution

We will now reduce the above PDE system to an ODE system by using the prescribed θ_s and θ_l profiles. This is accomplished by first integrating (over respective domains) each PDE and making use of the following Leibniz integral formula:

$$\frac{\partial}{\partial\lambda}\int_a^b f(x,\lambda)\,dx = f(b,\lambda)\,\frac{\partial b}{\partial\lambda} - f(a,\lambda)\,\frac{\partial a}{\partial\lambda} + \int_a^b \frac{\partial f}{\partial\lambda}dx \tag{11}$$

where λ is some parameter.

2.7. Solid Region

The Solid Region could be defined by using:

$$\Gamma_s = \int_1^\beta \theta_s(r^*,\tau)\,r^*dr^* \tag{12}$$

the HBI equation can then be obtained from Eq.(6) as:

$$\frac{1}{Ste}\left[\beta\frac{\partial\theta_s}{\partial r^*}(\beta,\tau) - \frac{\partial\theta_s}{\partial r^*}(1,\tau)\right] = \frac{\partial\Gamma_s}{\partial\tau} - \beta\frac{\partial\beta}{\partial\tau} \tag{13}$$

To simplify the above Eq.(13), we prescribe the following approximate temperature profile which satisfies the boundary conditions given by equations (6a) and (6b):

$$\theta_s = \frac{ln(r^*)}{In(\beta)} \tag{14}$$

Evaluating Eq.(12), we get

$$\Gamma_s = \frac{(1-\beta^2)}{4\,ln(\beta)} + \frac{\beta^2}{2} \tag{15}$$

Hence, it follows from Eq.(13) that

$$\frac{\partial\Gamma_s}{\partial\tau} = \beta\frac{\partial\beta}{\partial\tau} \tag{16}$$

By substituting for Γ_s from Eq.(15), we obtain

$$\left[\beta + \frac{\beta^2-1}{4\,\beta\,(ln(\beta))^2} - \frac{\beta}{2\,(ln(\beta))}\right]\frac{\partial\beta}{\partial\tau} = \beta\frac{\partial\beta}{\partial\tau} \tag{17}$$

This represents the simplified form of the HBI equation for the solid layer. Now, following Lardner and Pohle (1961), assume the following approximate temperature profile for the liquid region satisfying the corresponding boundary condition (Eqs.(9a)-(9c)):

$$\theta_l = \theta_l(r^*,\tau) = 1 - \left(\frac{\delta^*-r^*}{\delta^*-\beta}\right)\frac{ln\left(\frac{r^*}{\delta^*}\right)}{ln\left(\frac{\beta}{\delta^*}\right)} \tag{18}$$

We now need to determine the dimensionless solidification radius (β) and thermal penetration depth (δ^*) as a function of time (τ). Defining the ratio of two dimensionless thicknesses as

$$\Omega = \frac{\delta^*}{\beta} \tag{19}$$

We first evaluate the temperature derivative in the liquid and solid regions. Thus,

$$\frac{\partial\theta_l}{\partial r^*} \mid (r^*=\beta) = -\frac{1}{\beta}\frac{1}{ln\left(\frac{1}{\Omega}\right)} + \frac{1}{\beta\,(\Omega-1)} = \frac{1}{\beta\,(ln(\Omega))} + \frac{1}{\beta\,(\Omega-1)} \tag{20}$$

Similarly, the temperature gradient for the solid layer at the interface front can be written as:

$$\frac{\partial\theta_s}{\partial r^*} \mid (r^*=\beta) = \frac{1}{\beta\,(ln(\beta))} \tag{21}$$

Hence the interface condition Eq.(10) becomes

$$\beta\frac{\partial\beta}{\partial\tau} = \frac{1}{ln(\beta)} - K\phi\left[\frac{1}{ln(\Omega)} + \frac{1}{\Omega-1}\right] \tag{22}$$

Where K represents the thermal conductivity ratio given by $K = K_l/K_s$ and ϕ is the superheat defined in the Nomenclature section. Now, combining the simplified HBI for the solid layer (Eq.(17)) with the above simplified interface (Eq.(22)), we get

$$\left[\beta + \frac{\beta^2-1}{4\,\beta\,(ln(\beta))^2} - \frac{\beta}{2\,(ln(\beta))}\right]\frac{\partial\beta}{\partial\tau} = \frac{1}{ln(\beta)} - K\phi\left[\frac{1}{ln(\Omega)} + \frac{1}{\Omega-1}\right] \tag{23}$$

This represents the first main evolution equation to determine β. We need another equation to determine Ω to complete the mathematical specification of the physical problem.

2.8. Liquid Region

Solving the momentum equation Eq.(8) subject to boundary conditions in Eqs.(8a) and (8b), we get the following analytical solution for the velocity field:

$$V^* = a^*r^* - \frac{b^*}{r^*} \tag{24}$$

where a^* and b^* are constants given by:

$$a^* = \frac{\beta^2}{(\delta^*)^2-\beta^2} = \frac{-1}{\Omega^2-1} \tag{24a}$$

$$b^* = \frac{\beta^2}{(\delta^*)^2-\beta^2} = \frac{-\beta^2\Omega^2}{\Omega^2-1} \tag{24b}$$

Now, the HBI equation for the liquid can be obtained by integrating Eq.(9)as:

$$\underbrace{\int_\beta^{\delta^*}\frac{\partial}{\partial r^*}\left(r^*\frac{\partial\theta_l}{\partial r^*}\right)dr^*}_{C} + \underbrace{\int_\beta^{\delta^*}(Ec)(Pr)\,(r^*)^3\left[\frac{\partial}{\partial r^*}\left(\frac{V^*}{r^*}\right)\right]^2 dr^*}_{D} = \underbrace{\int_\beta^{\delta^*}\frac{\alpha_s}{\alpha_l}Ste\frac{\partial}{\partial\tau}(\theta_l\,r^*)\,dr^*}_{E} \tag{25}$$

We will consider each of the above terms separately and substitute the temperature and velocity profiles to integrate them.
Thus, we get

$$C = \int_{\beta}^{\delta^*} \frac{\partial}{\partial r^*}\left(r^* \frac{\partial \theta_l}{\partial r^*}\right) = -\beta \frac{\partial \theta_l}{\partial r^*}(\beta, \tau) \tag{26}$$

and

$$D = \int_{\beta}^{\delta^*} EcPr\,(r^*)^3 \left[\frac{\partial}{\partial r}\left(\frac{V^*}{r^*}\right)^2\right]^2 dr^* = 2(Ec)(Pr)\frac{\beta^2\Omega^2}{(\Omega^2-1)} \tag{27}$$

Defining the thermal diffusivity ratio as

$$\widetilde{\alpha} = \frac{\alpha_s}{\alpha_l} \tag{28}$$

and

$$\Gamma_l = \int_{\beta}^{\delta^*} \theta_l\,(r^*, \tau)\, r^* dr^* \tag{29}$$

we get

$$E = \widetilde{\alpha}(Ste)\int_{\beta}^{\delta^*} \frac{\partial}{\partial \tau}\left(\theta_l\, r^*\right) dr^* = \widetilde{\alpha}(Ste)\left[\frac{\partial \Gamma_l}{\partial \tau} - \delta^* \frac{\partial \delta^*}{\partial \tau}\right] \tag{30}$$

Evaluating Γ_l by using θ_l from Eq.(18) in Eq.(29), we get

$$\Gamma_l = \frac{1}{2}\beta^2\left(\Omega^2-1\right) + \frac{\beta^2}{(\Omega-1)\,ln\,(\Omega)} \left[\frac{1}{6}(3\Omega-2)\,ln\,(\Omega) - \frac{5}{36}\Omega^3 + \left(\frac{1}{4}\Omega - \frac{1}{9}\right)\right] \tag{31}$$

Defining a new term F as

$$F = \Gamma_l - \frac{1}{2}\Omega^2\beta^2 \tag{32}$$

and substituting for Γ_l from Eq.(32), leads to

$$F = \frac{\beta^2}{(\Omega-1)\,ln\,(\Omega)}\left[\frac{1}{6}(3\Omega-2)\,ln\,(\Omega) - \frac{5}{36}\Omega^3 + \left(\frac{1}{4}\Omega - \frac{1}{9}\right)\right] - \frac{1}{2}\beta^2 \tag{33}$$

Thus,we may rewrite the term E defined in Eq.(30) compactly as

$$E = \widetilde{\alpha}(Ste)\frac{\partial F}{\partial \tau} \tag{34}$$

Hence using Eqs. (26), (27),and (35) in Eq. (25), we finally obtain the HBI equation for the liquid regions region as

$$\widetilde{\alpha}(Ste)\frac{\partial F}{\partial \tau} = -\left[\frac{1}{ln(\Omega)} + \frac{1}{\Omega-1}\right] + 2(Ec)(Pr)\frac{\beta^2\Omega^2}{(\Omega^2-1)} \tag{35}$$

where F is given in Eq.(34).
Equation (35) represents the second main evolution in the system to determine β and Ω simultaneously given suitable initial conditions. Equations (22) and (35) can be integrated numerically using the standard fourth order Rung-Kutta method.

3. Results and Discussion

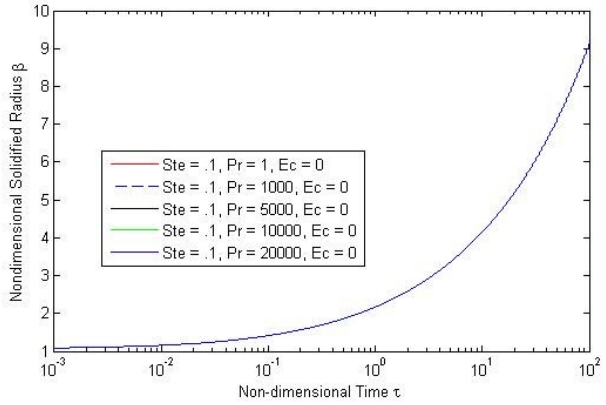

Figure 2:: The evolution of non-dimensional solidification front radius without rotation for different Prandtl numbers Pr

Fig.2 shows the evolution of the dimensionless solidification front radius β for different Prandtl numbers (Pr) without rotation $(Ec = 0)$ for Stefan number $Ste = 0.1$. It is seen that any variation in Pr does not affect the evolution of the frozen layer thickness.

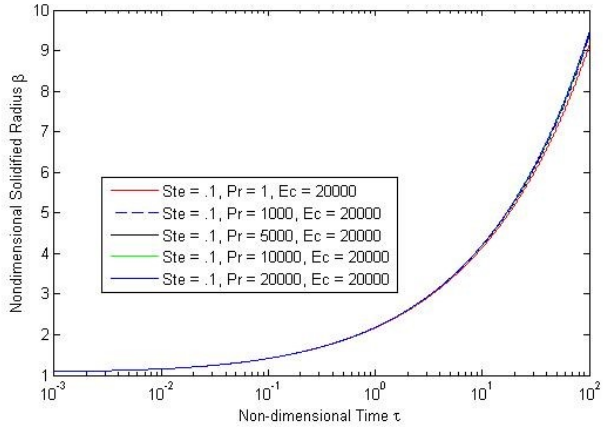

Figure 3:: The evolution of non-dimensional solidification front radius with rotation for different Prandtl numbers Pr

On the other hand, Fig.3 shows that when the cylinder is subjected to rotation, i.e. non-zero Eckert number (Ec=2000), increasing Pr tends to increase the solidification front radius β especially in the relatively later stage.

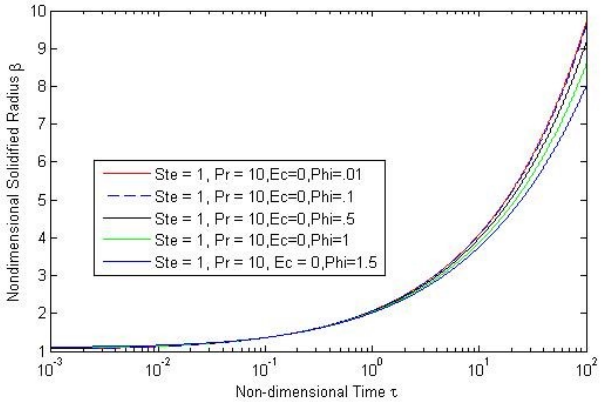

Figure 4:: The evolution of solidification radius without rotation for different superheat ratios

In Fig.4, the sensitivity of the evolution of the solidification front radius β with the superheat ratio ϕ for a stationary cylinder ($Ec = 0$) when $Ste = 1$ and $Pr = 10$ is demonstrated. It is evident that increasing ϕ results in higher solidification rates. For example, a 20% increasing in β at τ = 100 is seen when ϕ increases from 0.01 to 1.5.

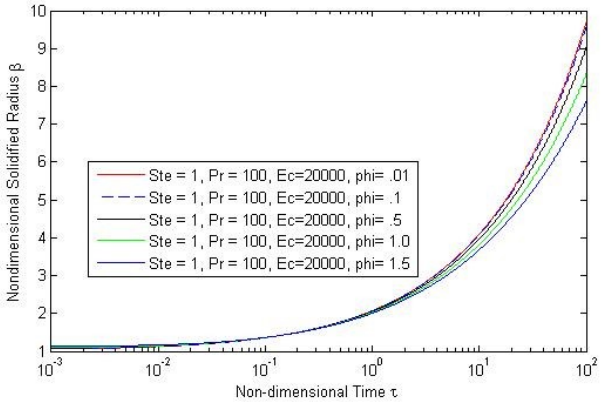

Figure 5:: The evolution of solidification radius with rotation for different superheat ratios

Figure 5 presents the effect of the superheat ratio $\phi$for a rotating cylinder with $Ec = 2000$. Again increasing ϕ causes a thicker frozen layer. For the conditions considered here, the effect of ϕ seems to be enhanced when the cylinder is subjected to rotation.

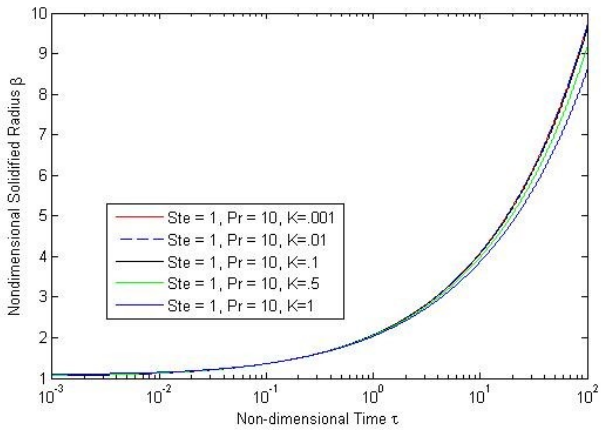

Figure 6:: The evolution of non-dimensional solidification front radius without rotation for different thermal conductivity ratios

The influence of the thermal conductivity ratio k on the solidification front over a stationary cylinder when $Ste = 1$ and $Pr = 10$ are shown in Fig.6. It is evident that unlike the superheat ratio case increasing k results in shorter solidification front radius.

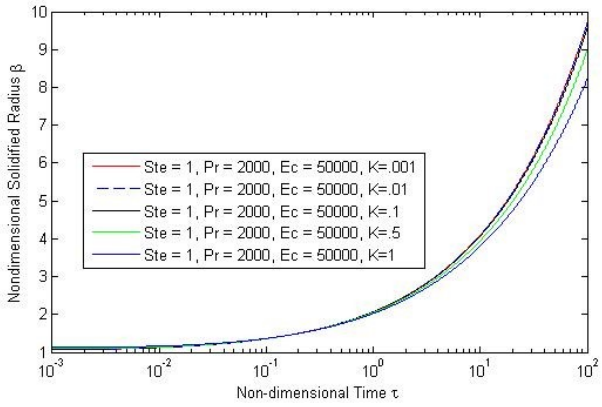

Figure 7:: The evolution of non-dimensional solidification front radius with rotation for different thermal conductivity ratios

Figure 7 presents the influence of the thermal conductivity ratio k, with the present case involving the rotation of the cylinder. Clearly, the difference between the case involving with and without rotation, when k is varied, is negligible.

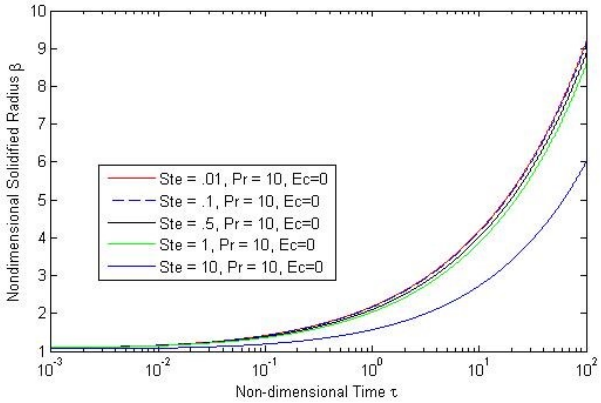

Figure 8:: The evolution of non-dimensional solidification front radius without rotation for different Stefan numbers

The effect of the Stefan number (Ste) on the solidification process over a stationary cylinder $(Ec = 0)$ when $Pr = 10$ is present in fig.8. It is found that when Ste is increasing, it results in a faster solidification rate. For example, when Ste changes from 0.01 to 10, the dimensionless solidification increasing by about 53%. It appears that Stefan number is one of the main characteristic parameters controlling the solidification process over a cylinder.

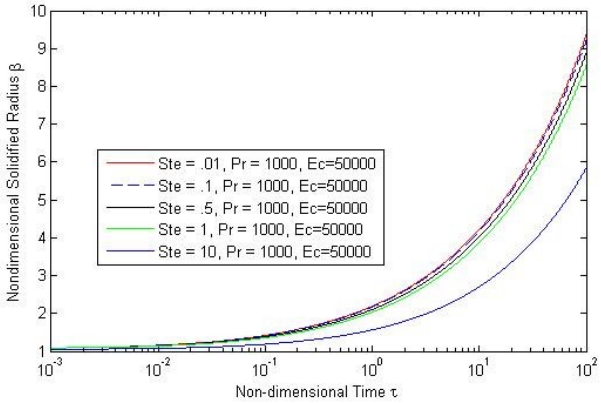

Figure 9:: The evolution of non-dimensional solidification front radius with rotation for different Stefan numbers

On the other hand, Fig.9 presents the influence of the Stefan number for a rotating cylinder $(Ec = 50000)$. It appears that whether the cylinder is stationary or rotating, the effect of Stefan number is the same with negligible quantitative differences.

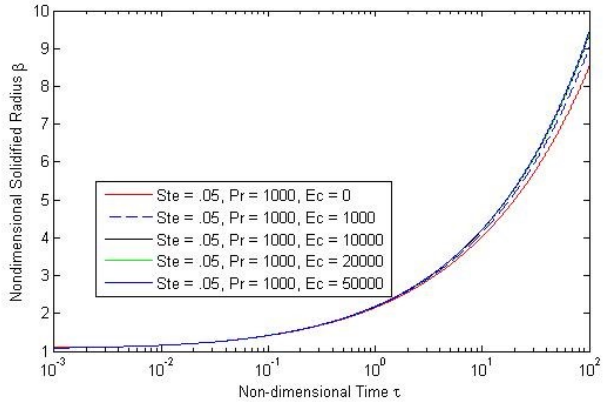

Figure 10:: The evolution of non-dimensional solidification front radius for different Eckert numbers

Finally, we will now present the effect of the change in the rotation rate, i.e. Ec on the evolution of the solidification front radius when $Ste = 0.05$ and $Pr = 1000$. As can be seen from Fig.10, increasing Ec causes a slower rate of solidification.

4. Summary and Conclusions

Phase change problems involving solidifications over a rotating cylinder have a number of applications in engineering related to manufacturing process involving casting of metals and plastics, and in large-scale ice production. While exact analytical solution is intractable for these problems, approximate methods or numerical approaches can be employed to perform fundamental investigations into the underlying basic phenomena. In this study a Heat Balance Integrate (HBI) method was applied to this problem. This reduced the more complex coupled conservation equations in the form of PDEs to a set of simplified ODEs. The resulting equations for the evaluation of the dimensionless solidification front radius as well as the thermal penetration radius were then solved numerically using the standard fourth order Runge-Kutta method. The following are the main conclusions of this study:

- Variations in the Prandtl numbers appear to have negligible influences on the solidification process, whether or not the cylinder is rotating.
- Increasing the superheat ratio ϕ results in faster solidification rates. For example, a 20% increase in the dimensionless solidification front radius β is seen when ϕ changes from 0.01 to 1.5.
- In contrast, it is found that increase in the thermal conductivity ratio k causes a shortening of the solidification front radius.
- The Stefan number Ste appears to be one of the main characteristic dimensionless groups controlling the solidification process. Increasing Ste is seen to cause faster rate of solidification. For example, when Ste is varied from 0.01 to 10, a 53% increase in the solidification front radius is seen.

- Finally, it is found that increasing the rotation rate or the Eckert number causes a shorter solidification front radius.

Recommendations

The following are some possible extensions of the present work that could be carried out in future studies:

- The present work considers the fluid undergoing solidification to be Newtonian. On the other hand, in many practical problems, the fluid can be of more complex nature and characterized to be non-Newtonian. Based on our derivation [12], the HBI solution of the solidification process over a rotating cylinder involving non-Newtonian fluids can be considered in a future study.
- The use of the HBI method in this work involves a number of underlying assumptions including prescribing the temperature profiles in each phase approximately. As such, the method is one-dimensional. In a future work, the various assumptions can be relaxed and full 2-D or 3-D numerical solutions can be obtained.
- Experimental investigation of the solidification process over a rotating cylinder for different fluids could complement the results obtained using the approximate analytical or numerical methods.

Nomenclature

α	Thermal diffusivity ratio
β	Dimensionless solidification radius,s/r_o
δ	Thermal penetration radius
δ^*	Dimensionless Thermal penetration radius,δ/r_o
Ω	Ratio of dimensionless thermal penetration radius and solidification front radius,δ^*/β
ϕ	Superheat ratio,$(T_o - T_i)/(T_i - T_w)$
τ	Dimensionless time,$\alpha_s\ Ste/r_o^2$
θ_l	Dimensionless liquid phase temperature, $(T_l - T_i)/(T_o - T_i)$
θ_s	Dimensionless solid phase temperature, $(T_s - T_w)/(T_i - T_w)$
Cps	Heat capacity of solid phase
Ec	Eckert number,$\omega^2 r_o^2/[Cp_l(T_o - T_i)]$
k	Thermal conductivity ratio,k_l/k_s
k_l	Thermal conductivity of liquid phase
k_s	Thermal conductivity of solid phase
L	Latent heat of fusion
Pr	Prandtl number,$\mu\ Cp_l/k_l$
r	Radial coordinate
r_o	Radial of cylinder
s	Radius of phase change location
Ste	Stefan Number,$Cps(T_i - T_w)/L$
T_i	Phase transition temperature
T_l	Liquid phase temperature
T_o	Initial temperature of q constant fluid
T_s	Solid phase temperature
T_w	Cylinder wall temperature
V	Fluid velocity
V^*	Dimensionless fluid velocity,$V/(wr_o)$

References

[1] Chatzimina M. et al, 2009 Wall Shear Rates Circular Couette Flow of a Herschel-Bulkey Fluid,*Applied Rheology*, 19,34228.

[2] Goodman,T.R, 1961 The Heat-Balance Integral and its Applications to problems Involving a change of phase,*Transactions of the **ASME***, 80,335-342.

[3] Goodman,T.R, 1961 The Heat-Balance Integral-Further Considerations and Refinements, *Journal of Heat Transfer*,83-85

[4] Goodman,T.R. and shea,J.J ,1960 The Melting of Finite Slabs,*Transactions of the **ASME***, 16-24.

[5] Hajabdillahi F., Premnath KN., Malepati S.,2018, "Effects of the Magnetic Field on Direct Contact Melting Transport Processes during Rotation"*Applied Mathematical modeling* (2018)61:421-442.

[6] Lardner, T.J. and Pohle, F.V,1961 Application of the Heat Balance Integral to problems of a cylindrical Geometry,*Transactions of the **ASME***, 83,310-312.

[7] Lunardini, V.J.,1981 Phase Change around a Circular Cylinder, *Journal of Heat Transfer*, 13,509-600.

[8] Mitchell, S.L., 2012, Applying the Combined Integral Method to One-dimensional Ablation,*Applied Mathematical Modeling*, 36, 127-138.

[9] Mitchell, S.L., Myers, T.G., 2010 Application of Slandered and Refined Heat Balance Integral Methods to one-dimensional System Problems,***SIAM** Reviews*, 52, 57-86.

[10] Mitchill, S.L., Myers, T.G., 2010 Improving the accuracy of heat balance integral methods applied to thermal problems with time dependent bounary coditions,*International journal of Heat and Mass Transfer*, 53,3540-3551

[11] Myers, T.G., Mitchell, S.L., Muchatibaya, G., Myers, M.Y.,2007, A cubic heat balance integral method for one-dimensional melting of a finite thickness layer,*International Journal of Heat and Mass transfer*, 50,5305-5317.

[12] Premnath, K.N,2013 Rotation Effect on Solidification Process Over a Cylinder Immersed in Non-Newtonian Fluids.

[13] Stewart Jr., W.E. and Smith,K.L,1987 Experimental Inward Solidification of Initially Superheat Water in a Cylinder *International Communication in Heat and Mass transfer*, 14,21-31.

[14] Wood, A.S,2001 A New Look at the Heat Balance Integral Method, *Applied mathematical modeling*, 25, 10.